Mammalian intestinal intracellular Microsporidia subvert host cell autophagy to promote replication

Johan Panek*, Kacper Sendra, Helen Glenwright, Gregor Kosta, Viktor I. Korolchuk*, Robert P. Hirt*

Address: Biosciences Institute, Faculty of Medical Sciences, Newcastle University, Newcastle upon Tyne, United Kingdom

*Corresponding authors: johan.panek@ncl.ac.uk, viktor.korolchuk@ncl.ac.uk, robert.hirt@ncl.ac.uk

Keywords: Microsporidia, Intracellular Parasite, Autophagy, *Encephalitozoon cuniculi*, RK-13 cells, CACO-2 cells, Gut mucosa.

Abstract

Intracellular pathogens such as Microsporidia can interact with host proteostasis pathways such as autophagy. Previous work done in *Caenorhabditis elegans* demonstrated involvement of autophagy in controlling Microsporidia proliferation through ubiquitin labelling of the parasite and subsequent degradation by autophagolysomes. However, it remains unknown if such mechanisms also play the role in mammalian models. Here we used immunochemistry assays, super-resolution confocal imaging, chemical and genetic modulation of the autophagy flux to elucidate the interplay between autophagy and Microsporidia in mammalian cells. We show that despite targeting by early autophagy markers (ubiquitin and p62); the host cell was not able to complete autophagy-mediated removal of *Encephalitozoon cuniculi*. Furthermore, instead of helping to control Microsporidia proliferation, the induction of autophagy dramatically increased proliferation of two microsporidia species in two different mammalian cell models. Finally, we showed that the reduction of the autophagy flux using siRNA treatment or microbiota-derived metabolites was able to reduce the parasite proliferation. Taken together our results indicate that Microsporidia infecting mammalian cells developed strategies to evade the host autophagy and, in contrast, can divert the autophagy flux to promote their own growth.

34 **Introduction**

35 Protein homeostasis is central to cellular physiology and ultimately to many aspects of health
36 and disease in humans (Taylor et al., 2014). Proteostasis relies on complex cellular regulatory
37 networks that include two major interconnected proteolytic degradation pathways: the
38 ubiquitin-proteasome system and the autophagy lysosome (autophagy) system (Klaips et al.,
39 2018). Genetic predispositions, ageing, infectious agents, and abiotic environmental factors
40 can all lead to dysregulation of these two pathways, which, in turn, underpins the pathobiology
41 of numerous conditions. This includes infectious (e.g. HIV), neurodegenerative (e.g.
42 Alzheimer's disease), chronic inflammatory conditions (e.g. inflammatory bowel diseases [IBD]
43 and rheumatoid arthritis), metabolic syndrome-associated diseases and cancers (Balch et al.,
44 2008).

45 Because they are building their ecological niche inside the host cell, intracellular pathogens
46 interact with host proteostasis, particularly with the autophagy pathway. Indeed, autophagy
47 can play a dual role in the survival of intracellular pathogens by both maintaining nutrient
48 balance of the host that can be diverted by the pathogen or by directly targeting intracellular
49 pathogens for degradation in a pathway called xenophagy (Sharma et al., 2018). As a result,
50 several of intracellular pathogens developed strategies to either escape this defence
51 mechanism or subvert it. This is best documented for intracellular bacterial pathogens such
52 as *Mycobacterium tuberculosis* or *Listeria spp.* that have developed specific
53 mechanisms/virulent factors to interfere with the maturation of the autophagosome, or
54 *Salmonella spp.* which secretes a deubiquitylation enzyme to remove its tagging by host
55 ubiquitin and thus can evade xenophagy altogether (Bach et al., 2008; Mitchell et al., 2015).
56 In contrast, far less is known about the intracellular eukaryotic parasites and their interaction
57 with host cell autophagy. However, their importance has been increasingly recognized in the
58 recent years, and studies had shown how some microbial parasites have developed strategies
59 to escape and take advantage of autophagy. For example, during its liver stages *Plasmodium*
60 *spp*. is targeted by host cell xenophagy as attested by rapid labelling of the meronts with host

61 LC3 and SQSTM1/p62 proteins (Schmuckli-Maurer et al., 2017). However, this targeting does
62 not lead to the engulfment of the parasite by canonical autophagosomes. Instead, it is located
63 in the structure that will eventually become the parasitophorous vacuole (PV), suggesting an
64 active recruitment of LC3 and a subversion of xenophagy by the parasite (Wacker et al., 2017).
65 This was confirmed by subsequent studies where induction of autophagy by either starvation
66 or rapamycin treatment in mice increased the parasite load of *Plasmodium berghei* (Prado et
67 al., 2015). Notably, in that same study, genetic suppression of autophagy through an *Atg5*
68 knock out, was both favouring an increase of pathogen load and reducing the size of the
69 parasites, illustrating the dual role of autophagy in both controlling the parasite and allowing it
70 to divert nutrients from the host cell for its own benefit (Prado et al., 2015).

71 Microsporidia is a group of highly diverse strict obligate intracellular pathogens, infecting most
72 animal lineages including economically and ecologically important species (Bateman et al.,
73 2016; Stentiford et al., 2016). Several species can infect humans and represent a significant
74 threat to immunocompromised patients (Mathis et al., 2005). Recent studies have also shown
75 that asymptomatic Microsporidia infections are more common in healthy immune-competent
76 individuals than previously thought (Sak et al., 2011) and may be associated with chronic
77 conditions including Crohn's disease and cancer (Andreu-Ballester et al., 2013; Leonard et
78 al., 2013). So far, the only study investigating the interaction between Microsporidia and
79 autophagy are available in the *Caenorhabditis elegans* model (Bakowski et al., 2014; Balla et
80 al., 2019). It was suggested that the Microsporidian species *Nematocida parisii* is targeted by
81 *C. elegans* xenophagy machinery in a CUL-6-dependent manner, leading to the labelling of
82 the parasite by host ubiquitin and LC3 (Bakowski et al., 2014). Knockdown of key autophagy
83 genes was sufficient to produce a moderate but significant increase of the parasite load. All
84 these results suggested that in the worm autophagy plays a role in controlling the infection
85 through the xenophagy pathway (Bakowski et al., 2014). In contrast, there are currently not
86 such data in the mammalian systems. In mammals, including humans, intestinal epithelium is
87 the main site of microsporidia infection (Stentiford et al., 2016). Perturbation of intestinal

88 autophagy, which was shown to be a major cause of intestinal disorder such IBDs or Crohn's
89 disease, was also linked to Microsporidia infection (Bretin et al., 2016; Hubbard and Cadwell,
90 2011). Therefore, investigating the interplay between mammalian cell autophagy and the
91 microsporidian species is of major interest.

92 We investigated this interplay using *E. cuniculi*, one of the most common microsporidia
93 species infecting mammals (Katinka et al., 2001). This species was originally isolated from
94 rabbit but is also commonly found in other mammals including humans. The diminutive *E.*
95 *cuniculi* genome is the results of massive genomic and protein coding capacity reduction (2.2
96 Mb encoding only 2,000 proteins) leading to the loss of multiple metabolic capabilities (Katinka
97 et al., 2001; Nakjang et al., 2013; Wadi and Reinke, 2020). These include the loss of numerous
98 biosynthesis pathways, and, notably, multiple genes mediating proteostasis, including the
99 mechanistic Target of Rapamycin (mTOR) pathway as well as the majority of the autophagy
100 machinery (Yang et al., 2017). This makes *E. cuniculi* an ideal model system to study the host
101 autophagy response to an eukaryotic intracellular pathogen. Previous transcriptomics
102 analyses found that, similar to *C. elegans,* rabbit kidney cells (RK-13) infected with
103 microsporidia *T. hominis* (Watson et al., 2015), were characterised by an upregulation of
104 genes tagged as key autophagy components (Bordi et al., 2021). While only *ATG4C* was
105 found to be significantly upregulated in the original dataset (*log^2 fold change*:1.59, adjusted *p-*
106 *value*:0.0025), 10 other genes had increased expression upon infection, including several key
107 *ATG* genes as well as 4 different Cullin genes, suggesting that autophagy/xenophagy may be
108 stimulated upon infection in the mammalian system (Watson et al., 2015). Here we exploited
109 a combination of antibodies developed to investigate *E. cuniculi* infections cycle (Tsaousis et
110 al., 2008), pharmacological treatments and genetic manipulation on mammalian cells to
111 investigate the interplay between Microsporidia infection and mammalian autophagy.

112

113 **Results**

114 ***E. cuniculi* co-localizes with p62 and ubiquitin suggesting its targeting by host cell**
115 **xenophagy machinery**

116 Xenophagy starts with the selective labelling of the pathogens by ubiquitin mediated by an E3
117 ubiquitin ligase. Ubiquitylation motifs are subsequently recognized by the UBA domain of the
118 receptor protein p62 which, after oligomerization, recruits the autophagy machinery through
119 its LC3-interacting region (LIR) leading to the engulfment of the parasite into an
120 autophagosome (Itakura and Mizushima, 2011). If microsporidia are targeted by xenophagy
121 in our model, co-localization of the parasite with ubiquitin, p62 and LC3 should be observed.
122 Indeed, previous studies in the *C. elegans* models showed a CUL-6-dependent ubiquitylation
123 of the early stages of the parasite as well as co-localization with the *C. elegans* LC3/ATG8
124 homolog (LGG-1) (Bakowski et al., 2014).

125 To verify if such mechanism was conserved in the mammalian model, we investigated co-
126 localization of p62 and conjugated ubiquitin (FK-2) with *E. cuniculi* meronts. The parasite was
127 labelled using an antibody made in a previous study (Tsaousis et al., 2008) which recognizes
128 one of the 4 nucleotide membrane transporters identified in *E. cuniculi* genome (E.c.NTT2).
129 This marker was selected because it is highly expressed during the whole *E. cuniculi* life cycle,
130 from the early meronts to the spore formation stages and also strongly labels the outside of
131 the PV (Fig S1).

132 Similar to what was seen in the *C. elegans* model, using super resolution confocal imaging
133 early meronts were found to be labelled by the conjugated ubiquitin antibody 6 hours post
134 infection (hpi) (Figure 1A-B). Interestingly, only the smaller parasite stages were labelled with
135 ubiquitin (Figure 1C) whereas labelling was never found on later stages suggesting that only
136 early meronts are targeted by xenophagy and degraded, preventing them to develop to further
137 stages. Another possibility could be that the parasite developed strategy to evade xenophagy
138 pathway by actively removing the ubiquitin labelling. To confirm the targeting of *E. cuniculi* by

139 host autophagy we used the same setup to assay the co-localization of the parasite with p62
140 and LC3 6 hpi. As expected, parasites were labelled with p62 (Figure 1C-E) however no co-
141 localization with LC3 was found. Therefore, our results suggest that *E. cuniculi* is targeted by
142 host cell xenophagy but is able to avoid being isolated into a fully matured autophagic vesicle.

143 *E. cuniculi* is a natural pathogen of a large range of mammals, where in most cases its infection
144 site is the intestinal epithelium. To confirm our results in a more physiologically-relevant model,
145 we performed the same experiments in human colorectal adenocarcinoma cells (CACO-2
146 cells) a common model system used to study pathogen-intestinal cell interactions . The results
147 were similar in this cell line with early meronts labelled with ubiquitin, and p62 (Figure 1F-I)
148 while no parasite labelled with LC3.

149 **Pharmacological induction of autophagy increases *E. cuniculi* proliferation**

150 If xenophagy was not relevant to clear Microsporidia infection in mammalian cells, induction
151 of autophagy should not reduce their proliferation rate. To assay microsporidia proliferation,
152 we used two metrics. First, a direct measure of the spore numbers produced per host cell 7
153 days post infection, and second, the size of the PV 48 hpi. This time point was chosen because
154 the first 2 days represent a growth latency phase during which the parasite only mildly
155 increases in size and starts to divide after 24 hpi. At 48 hpi the spore starts to be produced
156 and released at the centre of the PV, while the newly formed meronts labelled by the E.c.NTT2
157 antibody form a ring localized on the edge of the PV, allowing for the accurate measurement
158 of its surface (Figure 2A). The more spores are produced, the larger the PV become, so we
159 reasoned that comparing the size of the PV between different treatments should be a good
160 proxy to assay the successful proliferation of the parasite. To induce autophagy, we used torin-
161 1, a second-generation mTOR inhibitor which is known to be a very potent autophagy inducer
162 through direct inhibition of both mTORC1 and mTORC2 complexes (Liu et al., 2010).
163 However, due to its high potency, torin-1 has other side-effect such as promoting cell cycle
164 arrest, cells death and protein synthesis arrest (Moschetta et al., 2014). Hence to confirm that

165 the observed effect was due to autophagy induction the other natural mTOR inhibitor
166 rapamycin which only inhibits mTORC1 was also used (Moschetta et al., 2014).

167 Surprisingly, our results showed that instead of decreasing parasite proliferation both torin-1
168 and rapamycin increased it. With torin-1 treatment, the spore production per cell 7 dpi is
169 significantly increased, with a maximum reached at the lower tested dose (31 nM) with twice
170 more spores produced than with the DMSO control (Figure 2B-C). The size of the PV is also
171 significantly increased after the treatment with all doses of torin-1 with a maximum reached at
172 125 nM (Figure 2D). Cells treated with rapamycin showed a similar but milder effect with an
173 increase in spore production (Figure 2B, E) and in size of the PV (Figure 2F) for all but the 62
174 nM dose. These results suggest that autophagy appears to be beneficial to the parasite
175 proliferation instead of controlling it, confirming our previous results indicating that the parasite
176 is not being degraded by xenophagy. The discrepancy between torin-1 and rapamycin
177 treatment effect on parasite growth may be due to the difference in the potency of the drugs
178 to inhibit the mTOR pathway. These results also confirmed that size of the PV is a good proxy
179 to evaluate the efficiency of proliferation of the parasite and we decided to focus on this
180 measure in later experiments.

181 Next, we tested whether the ability of the parasite to take advantage of the host autophagy
182 pathway was conserved among different cell lines. Using a similar setup, we tested the effect
183 of the maximum dose of torin-1 (250 nM) on proliferation of *E. cuniculi* in CACO-2 cells. Once
184 again, the results confirmed that torin-1 treatment significantly increases both the number of
185 spores produced per cell and the size of the PV 48 hpi to an even more dramatic extent than
186 in RK-13 cells, with an increase of 300% in spore production compared to control (Figure 2G-
187 I).

188 Finally, we wondered if other Microsporidia species infecting mammals were able to benefit
189 from the host cell autophagy. Therefore, we investigated the effect of torin-1 treatment on the
190 growth of *Trachiopleiostophora hominis,* another species of Microsporidia originally isolated
191 from HIV patients and that we routinely cultivate in RK-13 cells (Field et al., 1996)(Heinz et al.

192 2014). The parasite was labelled with an antibody against T.h.NTT4, one of the 4 NTTs
193 identified in our previous study and which is expressed at high levels during the complete
194 lifecycle of the parasite (Heinz et al. 2014)(Dean et al., 2018). Our results showed a significant
195 increase in area of *the T. hominis* PV upon induction of autophagy by torin-1 treatment similar
196 to the data with *E. cuniculi* in RK-13 and CACO-2 cells (Figure 2J, K).

197 Taken together these results suggest that instead of controlling the proliferation, autophagy
198 activation in the host cell may benefit both *E. cuniculi* and *T. hominis* proliferation, as attested
199 by the increase in size of the PV and the number of spores produced per cell. This is consistent
200 with our previous results showing that xenophagy targeting of *E. cuniculi* was incomplete
201 (Figure 1). We hypothesized that *E. cuniculi* may have evolved a way to evade xenophagy
202 and, in contrast to be suppressed by it, exploit autophagy to derive nutrients from the host cell.
203 The fact that this phenomenon was observed in two different cell lines as well as with another
204 parasite species, suggested that this feature might be conserved across different
205 Microsporidia.

206 **Suppression of autophagy drastically reduces *E. cuniculi* proliferation**

207 Induction of autophagy with torin-1 and rapamycin is indeed a robust and well-characterized
208 approach but may also trigger other adverse effect such cell cycle arrest, protein synthesis
209 arrest and even cell death at higher dose. Hence, to validate our findings we investigated the
210 effect of autophagy inhibition using siRNA targeting a key autophagy gene *ATG5* on *E. cuniculi*
211 proliferation in the presence or absence of torin-1. To take advantage of reagents already
212 developed for human cells, we performed this experiment in CACO-2 cells.

213 To verify silencing efficiency, ATG5 abundancy, and LC3-II accumulation after Bafilomycin A1
214 treatment was assayed by immunoblotting in cells treated with either *ATG5* siRNA or non-
215 targeting siRNA (Figure 3A). The results revealed that despite a modest effect on ATG5 levels,
216 the silencing was sufficient to decrease LC3-II accumulation after Bafilomycin A1 treatment
217 by 58% suggesting a strong decrease in the autophagy flux (Figure 3B-C).

218 Confocal imaging of CACO-2 cells 48 hpi indicated that *ATG5* silencing significantly reduced
219 the size of *E. cuniculi* PV as well as the number of spores produced per cell in both torin-1 and
220 DMSO treated cells (Figure 3D-F). Interestingly, *ATG5* knockdown reverted the increase of
221 PV area in response to torin-1 treatment (Figure 3D-F). This observation supported the
222 hypothesis that increased PV size after torin-1 treatment is dependent on autophagy induction.
223 The increase in spore numbers in response to torin-1 treatment was also suppressed by *ATG5*
224 knockdown although only partially, which could be explained by these measurements done 7
225 dpi when the siRNA silencing effect may start to fade away.

226 **Repression of autophagy with the gut microbiota secondary metabolites reduces *E.***
227 ***cuniculi* proliferation**

228 Our results suggest that perturbation of the autophagy flux either due to genetic predisposition
229 such as in Crohn's Disease (CD), IBD or environmental factors such as microbiota, could have
230 an impact on the susceptibility to microsporidia infection. Interestingly, a previous study has
231 shown a higher prevalence of microsporidia infection in CD patients suggesting a potential
232 higher susceptibility to infection, especially to *E. cuniculi* (Andreu-Ballester et al., 2013).
233 Microbiota secondary metabolites can directly affect gut epithelium cell metabolism and
234 physiology. For example, exposure of CACO-2 cells to short chain fatty acids (SCFAs), which
235 are naturally produced by the intestinal microbiota in the presence of dietary fibres, has been
236 linked to a decrease in autophagy flux (Feng et al., 2018). Hence, we decided to investigate if
237 autophagy flux perturbation provoked by incubation with a mix of short chain fatty acids was
238 able to reduce *E. cuniculi* proliferation in CACO-2 cells.

239 For this experiment, we pre-treated CACO-2 cells with a mix of SCFA (acetate 0.5 mM,
240 butyrate 0.01 mM, and propionate 0.01 mM – as in (Feng et al., 2018)) for 48 h and then
241 infected them with *E. cuniculi,* maintaining the SCFA mix during the entire experiment. Our
242 results confirmed a significant decrease in the size of PV 48 hpi in SCFA treated cells vs
243 control treatment (Figure 4A-B). The number of spores produced per cell also had a trend for
244 reduction after SCFA treatment although did not reach significance (Figure 4C).

245 This result highlights the importance of gut epithelium homeostasis on the susceptibility to
246 infection by pathogens such as Microsporidia. Together, these results might also help to
247 explain the correlation between CD and Microsporidia prevalence seen in previous studies,
248 as CD patients are known to have dysfunction in the autophagy pathway (Larabi et al., 2020).

249

250 **Discussion**

251 Autophagy is a central pathway to respond to cytoplasmic stress, nutrient starvation, and
252 protein aggregation that are all potential outcomes of intracellular pathogen infections.
253 However, to date little has been done to study its involvement in the response of mammalian
254 cells to Microsporidia infection.

255 Here we found that *E. cuniculi* is partially labelled by the host autophagy markers. However,
256 the labelling of *E. cuniculi* by early autophagy markers is not followed by its engulfment into
257 LC3-decorated host cell autophagosome, suggesting that *E. cuniculi* is able to escape
258 xenophagy and avoid degradation. Further supporting our results, pharmacological induction
259 of autophagy using torin-1 or rapamycin treatment heavily increased parasite proliferation, as
260 attested by both the increase in spore production and size of the PV. Interestingly our results
261 with the other Microsporidia species *T. hominis* suggest that this beneficial effect of autophagy
262 induction on Microsporidia proliferation might be conserved among other Microsporidia
263 species and possibly other hosts. These results were corroborated by our siRNA experiments,
264 where knockdown of *ATG5* suppressed the parasite ability to multiply in the human cells.
265 Finally, we showed that microbiota secondary metabolites, namely a mix of 3 SCFA, were
266 able to negatively impact *E. cuniculi* multiplication in CACO-2 cells through what we
267 hypothesized to be a modulation of host cell autophagy. All these results suggest that in
268 contrast to the *C. elegans* model, the activation of autophagy in the mammalian cells is at least
269 inefficient, if not detrimental, to host cells to control the infection as it allowed for a more
270 effective parasite proliferation.

271 We propose that, unlike in *C. elegans* where autophagy may control Microsporidia infection,
272 Microsporidia infecting mammalian cells evolved means to escape autophagy and take
273 advantage of it to support their growth. Indeed, our results clearly indicate that in mammalian
274 cells *E. cuniculi* is able to escape xenophagy despite being labelled by both host ubiquitin and
275 p62, suggesting an evasion mechanism which will need to be elucidated in the future. A similar
276 escape from host xenophagy as well as the beneficial effect of autophagy induction has

277 previously been described for *Plasmodium berghei* infecting mice (Prado et al., 2015).
278 However, in the case of *Plasmodium*, xenophagy suppression (using *Atg5*$^{-/-}$ cell line) was
279 increasing the amount of parasite per cell while reducing their average PV size, suggesting
280 that xenophagy was able to partially control parasite proliferation. In our case, suppression of
281 xenophagy by *ATG5* knockdown in human cells was strongly reducing the PV size and the
282 parasite proliferation, suggesting that xenophagy might be ineffective in controlling the *E.*
283 *cuniculi* infection.

284 Autophagy pathway deregulation has been implicated in numerous pathologies including
285 IBDs, which were shown to present association with Microsporidia prevalence. Our study
286 might help to explain this association in some contexts, as perturbation in the autophagy
287 pathway could provoke a higher susceptibility to Microsporidia infection. It is also possible that
288 microsporidia infection will worsen IBD condition by further disturbing the autophagy flux of
289 the host cells. In conclusion, our study provides a novel mechanistic link between, on one side
290 the gut microbiota and parasites and on the other gut epithelium physiology and ultimately
291 human health.

292

293

294 **Methods**

295 Cell and parasite culture

296 RK-13 rabbit kidney cell line obtained from the ATCC (ATCC CCL-37) was grown at 37°C with
297 5% CO_2 in Dulbecco's Modified Eagle Medium (DMEM) (Gibco), containing 10% FBS (Gibco),
298 penicillin (100 µg/ml), streptomycin (100 µg/ml), kanamycin (100 µg/ml), and Fungizone (1
299 µg/ml) purchased from Sigma. CACO-2 cells line obtained from ATCC (ATCC HTB-37) was
300 grown at 37℃ in complete Modified Eagle Medium (MEM) medium complemented with 20%
301 FBS, penicillin (100 µg/ml) streptomycin (100 µg/ml), kanamycin (100 µg/ml) and Fungizone
302 (1 µg/ml). The microsporidia *E. cuniculi* EC2 and *T. hominis* (ATCC PRA-404) were routinely
303 subcultured in RK-13 cells grown as previously described (Tsaousis et al., 2008). Spores used
304 in time course experiments were harvested from infected RK-13 cells grown in 175 cm^2 flasks.
305 Cells were washed and scraped in phosphate buffer saline (PBS) and then lysed by 3
306 passages through a 25G needle and 3 rounds of 1 min sonication on ice. Released spores
307 were purified by layering onto a 25% Percoll gradient and centrifugation at 900 g for 30 min.
308 After 3 washes in PBS, the pelleted spores were resuspended in PBS and used within a week
309 to infect RK-13 or CACO-2 cells.

310 Time course experiments

311 RK-13 cells or CACO-2 cells were seeded into 24-well (for protein extraction) or 6-well plates
312 (for immunofluorescence and spore production assays). When confluent, purified spores were
313 added with a multiplicity of infection of 200. After 30 min the cells were washed 2 times with
314 medium and fresh medium with or without treatment was added (torin-1 31-250 nM *Selleck*
315 *Chemicals*, rapamycin 12.5-250 nM *Selleck Chemicals*, SCFA mix (acetate 0.5 mM, butyrate
316 0.01 mM, and propionate 0.01 mM) *Sigma-Aldrich*, DMSO, PBS). Medium was changed every
317 3 days and treatment was maintained for the full duration of the experiment.

318 Spore production assay

319 7 dpi, cells were washed 2 times with PBS, and detached with trypsin. Part of the cell
320 suspension was used to quantify the number of cells per well. The remaining suspension was
321 centrifuged for 5 min at 16,000 g, the pellet was resuspended in RIPA buffer with 1% SDS.
322 The lysate was sonicated for 1 min at 4℃ to reduce the viscosity and centrifuged for 5 min at
323 16,000g. The pelleted spores were then resuspended in PBS and counted on Neubauer
324 counting chamber. All assays were done in 3 independent biological triplicates. Spores
325 produced per cell were then calculated and plotted in GraphPad Prism.

326 Immunofluorescence assays

327 6-, 48- or 72-hours post infections, coverslips were washed 3 times with PBS, and fixed for 15
328 min with ice-cold 50% methanol, 50% acetone. The coverslips were later rehydrated in PBS
329 for 15 min, blocked in PBS 3% milk and labelled with primary antibodies diluted in blocking
330 buffer overnight at 4℃ in humid chamber (mouse α-conjugated ubiquitin - 1:100: *BML-*
331 *PW8810-0100 - Enzo life science*, mouse α-p62 - 1:100: *#88588 - Cell Signalling Technology*,
332 rat α-E.c.NTT2 1:200 – [Tsaousis et al., 2008], rabbit α-E.c.HSP70 1:500 – [Tsaousis et al.,
333 2008], rabbit α-T.h.NTT4 1:200 – [Dean et al., 2018], rat α-T.h.HSP70 1:500 – [Dean et al.,
334 2018]). After 3 washes in PBS, coverslips were labelled for 2 h at room temperature with
335 secondary antibodies (α-rat Alexa fluor 488, α-rabbit Alexa fluor 568, α-rabbit Alexa fluor 594
336 - *Invitrogen*) then washed again 3 times in PBS, counterstained with DAPI and mounted on
337 slides with Prolong glass antifade mounting solution. For co-localisation assays the slides
338 were imaged with a 63X magnification on a Zeiss LSM800 confocal microscope using airyscan
339 super-resolution mode. The red and green signals were then quantified over a transect using
340 ImageJ and intensity values were plotted using GraphPad Prism. For kinetic of infection
341 experiments, the slides were imaged using a Zeiss AxioImager with a 63X magnification. For
342 each condition images were taken randomly on 3 slides using the same acquisition
343 parameters across each set of experiments. The images were then blinded using a home-
344 made python script and the measurement of the parasitophorous vacuoles was done using a
345 home-made ImageJ macro. Briefly, the colour channels were split, the channel containing

346 NTT2 signal was then manually thresholded to separate NTT2 signal from background, the
347 resulting binary image was then used to automatically detect PV using ImageJ detect particles
348 tools. The resulting regions of interest were then measured and saved in a zip file. For each
349 condition and experiment at least 30 PV were measured.

350 Immunoblotting

351 4 h before sampling, Bafilomycin A1 was added in the medium at a final concentration of 400
352 nM. While on ice, cells were washed twice with ice cold PBS and scrapped on ice in ice-cold
353 RIPA buffer (*Sigma-Aldrich*) with complete Protease Inhibitor Cocktail (*Roche*). After 15 min
354 on ice, cells lysates were centrifuged for 15 min at 16,000g 4℃ and supernatant protein
355 concentration was determined using BCA Protein Assay (*Pierce*). Protein samples were mixed
356 with 4x Laemmli Sample Buffer at a final protein concentration of 5 µg/µl for each sample. 75
357 µg of proteins were separated on 15% SDS-PAGE gel and transferred on 0.2 µm pore size
358 PVDF membrane. After a blocking step in TBST, 5% milk, membranes were incubated in
359 primary antibodies diluted in TBST, 3% BSA overnight at 4℃ (rabbit α-LC3B 1:1000 – *Cell*
360 *Signaling/ #4108*, rabbit α-Atg5 1:1000 – *Cell Signaling/#2630*, mouse α-tubulin 1:1000 –
361 *Sigma Aldrich/T5168*). After 3 washes in TBST the membranes were incubated in secondary
362 antibodies for 2 h at room temperature (Goat α-rabbit HRP 1:1000 - *Sigma Aldrich/*
363 *GERPN4301*, Goat α-mouse HRP 1:1000– *Sigma Aldrich/GERPN4401*), revealed using ECL
364 reagent (BioRad) and signal was acquired on a BioRad Bioimager. Quantification was done
365 using gel quantification tool in ImageJ.

366 siRNA

367 ON-TARGETplus SMARTpool siRNA against human *ATG5* (L-004374-00-0005) and
368 nontargeting SMARTpool siRNA (D-001810-10-05) were purchased from *Horizon Discovery*.
369 Silencing was done in two steps, a first transfection with a final siRNA concentration of 100
370 nM was done for 24 h in a 6-well plate, followed by a passaging of the transfected cells into
371 24-well plate. 24 h after plating, the cells were transfected second time with a final

372 concentration of 20 nM siRNA. 24 h after the second treatment cells were infected and treated
373 with torin-1 (250 nM) or DMSO as a control.

374

375 Statistical analyses

376 GraphPad Prism version 9.00 was used for statistical analyses and statistical presentation of
377 quantitation. *P-values* are presented in the figures above the compared conditions: *** P <
378 0.001, ** P < 0.01, * P<0.05. Where two conditions were compared, a paired two-tailed
379 Student's t test was used (Figures 2H, 2I). If more than two conditions were compared, a one-
380 way ANOVA followed by a Sidak's multiple comparisons test was applied (Figures 2C, 2D,
381 2E, 2F, 2K, 4B, 4C). For grouped data, a 2-way ANOVA followed by a Tukey's multiple
382 comparisons was applied (Figures 3E, 3F).

383

384 **Acknowledgements:** We are grateful to Newcastle Bioimaging Unit for imaging assistance.

385 **Funding:** This study was supported by the European Union's Horizon 2020 research and
386 innovation programme (Marie Skłodowska-Curie Grant Agreements No. 97617) to J.P.;
387 BBSRC (BB/M023389/1) and BBSRC (BB/R008167/2) to V.I.K.

388 **Author Contributions:** JP, RPH, VIK designed research; JP, KS, GK performed experiments;
389 JP, KS contributed new reagents or analytic tools; JP analysed data and wrote the manuscript;
390 RPH, VIK edited and proofread the text.

391 **Competing interests:** All authors declare they have no competing interests.

392

393

394 **References**

395 Andreu-Ballester JC, Garcia-Ballesteros C, Amigo V, Ballester F, Gil-Borrás R, Catalán-Serra
396 I, Magnet A, Fenoy S, del Aguila C, Ferrando-Marco J, Cuéllar C. 2013. Microsporidia
397 and its relation to Crohn's disease. A retrospective study. *PLoS One* **8**:e62107.
398 doi:10.1371/journal.pone.0062107

399 Bach H, Papavinasasundaram KG, Wong D, Hmama Z, Av-Gay Y. 2008. Mycobacterium
400 tuberculosis Virulence Is Mediated by PtpA Dephosphorylation of Human Vacuolar
401 Protein Sorting 33B. *Cell Host & Microbe* **3**:316–322. doi:10.1016/J.CHOM.2008.03.008

402 Bakowski MA, Desjardins CA, Smelkinson MG, Dunbar TL, Lopez-Moyado IF, Rifkin SA,
403 Cuomo CA, Troemel ER. 2014. Ubiquitin-Mediated Response to Microsporidia and Virus
404 Infection in *C. elegans*. *PLoS Pathogens* **10**:e1004200.
405 doi:10.1371/journal.ppat.1004200

406 Balch WE, Morimoto RI, Dillin A, Kelly JW. 2008. Adapting Proteostasis for Disease
407 Intervention. *Science* **319**:916–9. doi:10.1126/science.1141448

408 Balla KM, Lažetić V, Troemel ER. 2019. Natural variation in the roles of *C. elegans* autophagy
409 components during microsporidia infection. *PLoS ONE* **14**.
410 doi:10.1371/journal.pone.0216011

411 Bateman KS, Wiredu-Boakye D, Kerr R, Williams BAP, Stentiford GD. 2016. Single and multi-
412 gene phylogeny of *Hepatospora* (Microsporidia) - a generalist pathogen of farmed and
413 wild crustacean hosts. *Parasitology* 1–12. doi:10.1017/S0031182016000433

414 Bordi M, de Cegli R, Testa B, Nixon RA, Ballabio A, Cecconi F. 2021. A gene toolbox for
415 monitoring autophagy transcription. *Cell Death & Disease 2021 12:11* **12**:1–7.
416 doi:10.1038/s41419-021-04121-9

417 Bretin A, Carrière J, Dalmasso G, Bergougnoux A, B'chir W, Maurin AC, Müller S, Seibold F,
418 Barnich N, Bruhat A, Darfeuille-Michaud A, Nguyen HTT. 2016. Activation of the

419 EIF2AK4-EIF2A/eIF2α-ATF4 pathway triggers autophagy response to Crohn disease-
420 associated adherent-invasive Escherichia coli infection. *Autophagy* **12**:770–783.
421 doi:10.1080/15548627.2016.1156823

422 Dean P, Sendra KM, Williams TA, Watson AK, Major P, Nakjang S, Kozhevnikova E, Goldberg
423 A v., Kunji ERS, Hirt RP, Embley TM. 2018. Transporter gene acquisition and innovation
424 in the evolution of Microsporidia intracellular parasites. *Nature Communications* **9**:1–12.
425 doi:10.1038/s41467-018-03923-4

426 Feng Y, Wang Y, Wang P, Huang Y, Wang F. 2018. Short-Chain Fatty Acids Manifest
427 Stimulative and Protective Effects on Intestinal Barrier Function Through the Inhibition of
428 NLRP3 Inflammasome and Autophagy. *Cellular Physiology and Biochemistry* **49**:190–
429 205. doi:10.1159/000492853

430 Field AS, Marriott DJ, Milliken ST, Brew BJ, Canning EU, Kench JG, Darveniza P, Harkness
431 JL. 1996. Myositis associated with a newly described microsporidian, Trachipleistophora
432 hominis, in a patient with AIDS. *Journal of Clinical Microbiology* **34**:2803–2811.

433 Grisdale CJ, Bowers LC, Didier ES, Fast NM. 2013. Transcriptome analysis of the parasite
434 *Encephalitozoon cuniculi*: An in-depth examination of pre-mRNA splicing in a reduced
435 eukaryote. *BMC Genomics* **14**. doi:10.1186/1471-2164-14-207

436 Hubbard VM, Cadwell K. 2011. Viruses, autophagy genes, and Crohn's disease. *Viruses*
437 **3**:1281–311. doi:10.3390/v3071281

438 Itakura E, Mizushima N. 2011. p62 targeting to the autophagosome formation site requires
439 self-oligomerization but not LC3 binding. *Journal of Cell Biology* **192**:17–27.
440 doi:10.1083/jcb.201009067

441 Katinka MD, Duprat S, Cornillot E, Metenier G, Thomarat F, Prensier G, Barbe V, Peyretaillade
442 E, Brottier P, Wincker P, Delbac F, el Alaoui H, Peyret P, Saurin W, Gouy M,
443 Weissenbach J, Vivares CP. 2001. Genome sequence and gene compaction of the

444 eukaryote parasite *Encephalitozoon cuniculi*. *Nature* **414**:450–453.
445 doi:http://www.nature.com/nature/journal/v414/n6862/suppinfo/414450a0_S1.html

446 Klaips CL, Jayaraj GG, Hartl FU. 2018. Pathways of cellular proteostasis in aging and disease.
447 *Journal of Cell Biology*. doi:10.1083/jcb.201709072

448 Larabi A, Barnich N, Nguyen HTT. 2020. New insights into the interplay between autophagy,
449 gut microbiota and inflammatory responses in IBD. *Autophagy* **16**:38–51.
450 doi:10.1080/15548627.2019.1635384

451 Leonard CA, Schell M, Schoborg RV, Hayman JR. 2013. *Encephalitozoon intestinalis* infection
452 increases host cell mutation frequency. *Infectious Agents and Cancer* **8**:43.
453 doi:10.1186/1750-9378-8-43

454 Liu Q, Chang JW, Wang J, Kang SA, Thoreen CC, Markhard A, Hur W, Zhang J, Sim T,
455 Sabatini DM, Gray NS. 2010. Discovery of 1-(4-(4-propionylpiperazin-1-yl)-3-
456 (trifluoromethyl)phenyl)-9-(quinolin-3-yl)benzo[h][1,6]naphthyridin-2(1H)-one as a highly
457 potent, selective Mammalian Target of Rapamycin (mTOR) inhibitor for the treatment of
458 cancer. *J Med Chem* **53**:7146. doi:10.1021/JM101144F

459 Mathis A, Weber R, Deplazes P. 2005. Zoonotic potential of the microsporidia. *Clinical*
460 *Microbiology Reviews*. doi:10.1128/CMR.18.3.423-445.2005

461 Mitchell G, Ge L, Huang Q, Chen C, Kianian S, Roberts MF, Schekman R, Portnoy DA. 2015.
462 Avoidance of Autophagy Mediated by PlcA or ActA Is Required for Listeria
463 monocytogenes Growth in Macrophages. *Infection and Immunity* **83**:2175.
464 doi:10.1128/IAI.00110-15

465 Moschetta M, Reale A, Marasco C, Vacca A, Carratù MR. 2014. Therapeutic targeting of the
466 mTOR-signalling pathway in cancer: benefits and limitations. doi:10.1111/bph.12749

467 Nakjang S, Williams TA, Heinz E, Watson AK, Foster PG, Sendra KM, Heaps SE, Hirt RP,
468 Martin Embley T. 2013. Reduction and expansion in microsporidian genome evolution:

469 new insights from comparative genomics. *Genome Biol Evol* **5**:2285–2303.
470 doi:10.1093/gbe/evt184

471 Prado M, Eickel N, de Niz M, Heitmann A, Agop-Nersesian C, Wacker R, Schmuckli-Maurer
472 J, Caldelari R, Janse CJ, Khan SM, May J, Meyer CG, Heussler VT. 2015. Long-term live
473 imaging reveals cytosolic immune responses of host hepatocytes against plasmodium
474 infection and parasite escape mechanisms. *Autophagy* **11**:1561–1579.
475 doi:10.1080/15548627.2015.1067361/SUPPL_FILE/KAUP_A_1067361_SM0752.ZIP

476 Sak B, Kváč M, Kučerová Z, Květoňová D, Saková K. 2011. Latent microsporidial infection in
477 immunocompetent individuals - a longitudinal study. *PLoS Neglected Tropical Diseases*
478 **5**:1–5. doi:10.1371/journal.pntd.0001162

479 Schmuckli-Maurer J, Reber V, Wacker R, Bindschedler A, Zakher A, Heussler VT. 2017.
480 Inverted recruitment of autophagy proteins to the Plasmodium berghei parasitophorous
481 vacuole membrane. *PLOS ONE* **12**:e0183797. doi:10.1371/JOURNAL.PONE.0183797

482 Sharma V, Verma S, Seranova E, Sarkar S, Kumar D. 2018. Selective Autophagy and
483 Xenophagy in Infection and Disease. *Frontiers in Cell and Developmental Biology* **6**:147.
484 doi:10.3389/FCELL.2018.00147

485 Stentiford GD, Becnel JJ, Weiss LM, Keeling PJ, Didier ES, Williams BAP, Bjornson S, Kent
486 ML, Freeman MA, Brown MJF, Troemel ER, Roesel K, Sokolova Y, Snowden KF, Solter
487 L. 2016. Microsporidia - Emergent Pathogens in the Global Food Chain. *Trends Parasitol*
488 **32**:1–13. doi:10.1016/j.pt.2015.12.004

489 Taylor RC, Dillin A, Colby DW, Prusiner SB, Finkbeiner S, Chen B, Retzlaff M, Roos T, Taylor
490 RC, Dillin A, Taylor RC, Dillin A. 2014. Aging as an Event of Proteostasis Collapse **1**:1–
491 17. doi:10.1101/cshperspect.a004440

492 Tsaousis AD, Kunji ERS, Goldberg A v, Lucocq JM, Hirt RP, Embley TM. 2008. A novel route
493 for ATP acquisition by the remnant mitochondria of *Encephalitozoon cuniculi*. *Nature*
494 **453**:553–556. doi:10.1038/nature06903

495 Wacker R, Eickel N, Schmuckli-Maurer J, Annoura T, Niklaus L, Khan SM, Guan JL, Heussler
496 VT. 2017. LC3-association with the parasitophorous vacuole membrane of Plasmodium
497 berghei liver stages follows a noncanonical autophagy pathway. *Cellular Microbiology*
498 **19**:e12754. doi:10.1111/CMI.12754

499 Wadi L, Reinke AW. 2020. Evolution of microsporidia: An extremely successful group of
500 eukaryotic intracellular parasites. *PLOS Pathogens* **16**:e1008276.
501 doi:10.1371/JOURNAL.PPAT.1008276

502 Watson AK, Williams TA, Williams BAP, Moore KA, Hirt RP, Embley TM. 2015. Transcriptomic
503 profiling of host-parasite interactions in the microsporidian Trachipleistophora hominis.
504 *BMC Genomics* **16**:1–20. doi:10.1186/s12864-015-1989-z

505 Yang J, Chai XQ, Zhao XX, Li X. 2017. Comparative genomics revealed the origin and
506 evolution of autophagy pathway. *Journal of Systematics and Evolution* **55**:71–82.
507 doi:10.1111/JSE.12212

508

509

510

511 **Figure Legends**

512 **Figure 1.** (*A, C, D*) Confocal super resolution imaging of RK-13 cells 48 hpi by *E. cuniculi*.
513 Parasite PV is labelled in green with α-E.c.NTT2 and in purple with α-HSP70, ubiquitin or p62
514 are in red. Yellow line indicates transect used for graph B and E. *(B, E)* Plot of the intensity
515 value for green and red signal over a transect indicated in figures A, C and D. (F, H) Confocal
516 super resolution imaging of CACO-2 cells 48 hpi by *E. cuniculi*. Parasite PV is labelled in green
517 with α-E.c.NTT2, ubiquitin or p62 in red. Yellow line indicates transect used for graph G and
518 I. *(G, I)* Plot of the grey value for green and red signal over a transect indicated in figures F
519 and H.

520 **Figure 2.** Chemical induction of autophagy increases PV area in RK-13 cells and CAOC-2
521 cells. *(A)* Fluorescence imaging of RK-13 cell at different time points post infection by *E.*
522 *cuniculi*, from 6 to 72 hpi. Parasite PV is labelled in green with α-E.c.NTT2 and in red with α-
523 HSP70. PV is highlighted by dashed line and area in μm^2 measured with ImageJ is indicated
524 on every picture. *(B)* Representative fluorescence imaging of RK-13 cells 48 hpi by *E. cuniculi*
525 in the presence of increasing doses of torin-1 or rapamycin. Parasite PV is labelled in green
526 with α-E.c.NTT2 and in red with α-HSP70. In each picture a representative PV is highlighted
527 with dashed line and the average area of the PV for this condition is indicated. *(C and E)* Graph
528 indicating the number of *E. cuniculi* spores produced per RK-13 cells 7 dpi with different
529 concentrations of torin-1 or rapamycin. 3 independent biological replicates per point, error bars
530 indicate SD. *(D and F)* Graph showing areas of the PV measured in different treatments. Mean
531 area of the replicates is indicated by black bar with errors bars as SD. Each dot represents
532 one measure. At least 30 measurements per condition were done. (G) Representative
533 fluorescence imaging of CACO-2 cells 48 hpi by *E. cuniculi* in presence of 250 nM torin-1 or
534 DMSO. Parasite PV is labelled in green with α-E.c.NTT2 and in red with α-HSP70. In each
535 picture a representative PV is highlighted with dashed line and the average area of the PV for
536 this condition is indicated. *(H)* Graph indicating the number of *E. cuniculi* spores produced per
537 CACO-2 cells 7 dpi with 250 nM torin-1 or DMSO. 3 independent biological replicates per

538 point, error bars indicate SD. *(I)* Areas of the PV measured in the 2 different treatments. Mean
539 area of the replicates is indicated by black bar with error bars as SD. Each dot represents one
540 measure. At least 30 measurements per condition were done. *(J)* Representative fluorescence
541 imaging of RK-13 cells 72 hpi by *T. hominis* in the presence of increasing doses of torin-1.
542 Parasite PV is labelled in red with α-T.h.NTT4 and in green with α-HSP70. In each picture a
543 representative PV is highlighted with dashed line and the average area of the PV for each
544 condition is indicated. *(K)* Graph showing areas of the PV measured in different treatments.
545 Mean area of the replicates is indicated by black bar with errors bars as SD. Each dot
546 represents one measure.

547 **Figure 3**. Silencing of ATG5 by siRNA treatment reduces *E. cuniculi* proliferation in CACO-2
548 cells. *(A)* Western blot of LC3-II, ATG5 and tubulin (loading control) after ATG5 siRNA
549 treatment of CACO-2 cells. *(B)* Quantification of ATG5 abundance from western blot shown in
550 A. *(C)* Quantification of LC3-II accumulation shown in western blot A. *(D)* Representative
551 fluorescence imaging of RK-13 cells 48 hpi by *E. cuniculi* in the presence in presence or
552 absence of torin-1 (250 nM) and with or without ATG5 siRNA treatment. In each image, a
553 representative PV is highlighted with dashed line and the average area of the PV for this
554 condition is indicated. *(E)* Graph showing areas of the PV measured in the different treatments.
555 Mean area of the replicates is indicated by black bar with errors bars as SD. Each dot
556 represents one measure. *(F)* Graph indicating the number of *E. cuniculi* spores produced per
557 RK-13 cell 7 dpi with different treatments. 3 independent biological replicates per point, error
558 bars indicate SD.

559 **Figure 4.** SCFA mix treatment reduces *E. cuniculi* proliferation in RK-13 cells.
560 *(A)* Representative fluorescence imaging of RK-13 cells 48 hpi by *E. cuniculi* in the presence
561 of 250 nM torin-1, SCFA mix or PBS. In each picture, a representative PV is highlighted with
562 dashed line and the average area of the PV for this condition is indicated. *(C)* Graph showing
563 areas of the PV measured in the different treatments. Mean area of the replicates is indicated
564 by black bar with errors bars as SD. Each dot represents one measure. *(D)* Graph indicating

565 the number of *E. cuniculi* spores produced per RK-13 cell 7 dpi with the different treatments.
566 3 independent biological replicates per point, error bars indicate SD.

567

568 **Supplementary Figure 1.** NTT2 transporter is expressed during the whole length of *E.*
569 *cuniculi* life cycle by meronts localised on the edge of the PV. *(A)* Expression level of NTTs
570 transcript during the *E. cuniculi* time course experiment (data from Grisdale et al., 2013) Km
571 for each of the nucleotide transporter are indicated on the graph (Tsaousis et al., 2008). *(B)*
572 Early meronts labelled with NTT1, NTT2 or NTT4 antibodies. NTT2 antibodies label the
573 periphery of the PV alongside the membrane (white arrowheads). Sporonts (white arrows)
574 labelled with NTT3 antibodies were localized closer to the centre of the vesicle. NTT4
575 antibodies label small sub-population of cells observed in large PVs corresponding to the late
576 stage of infection but not in any of the time points in the time course experiment. Spores
577 (orange arrowheads) were not labelled with any of the antibodies tested.

Figure 1

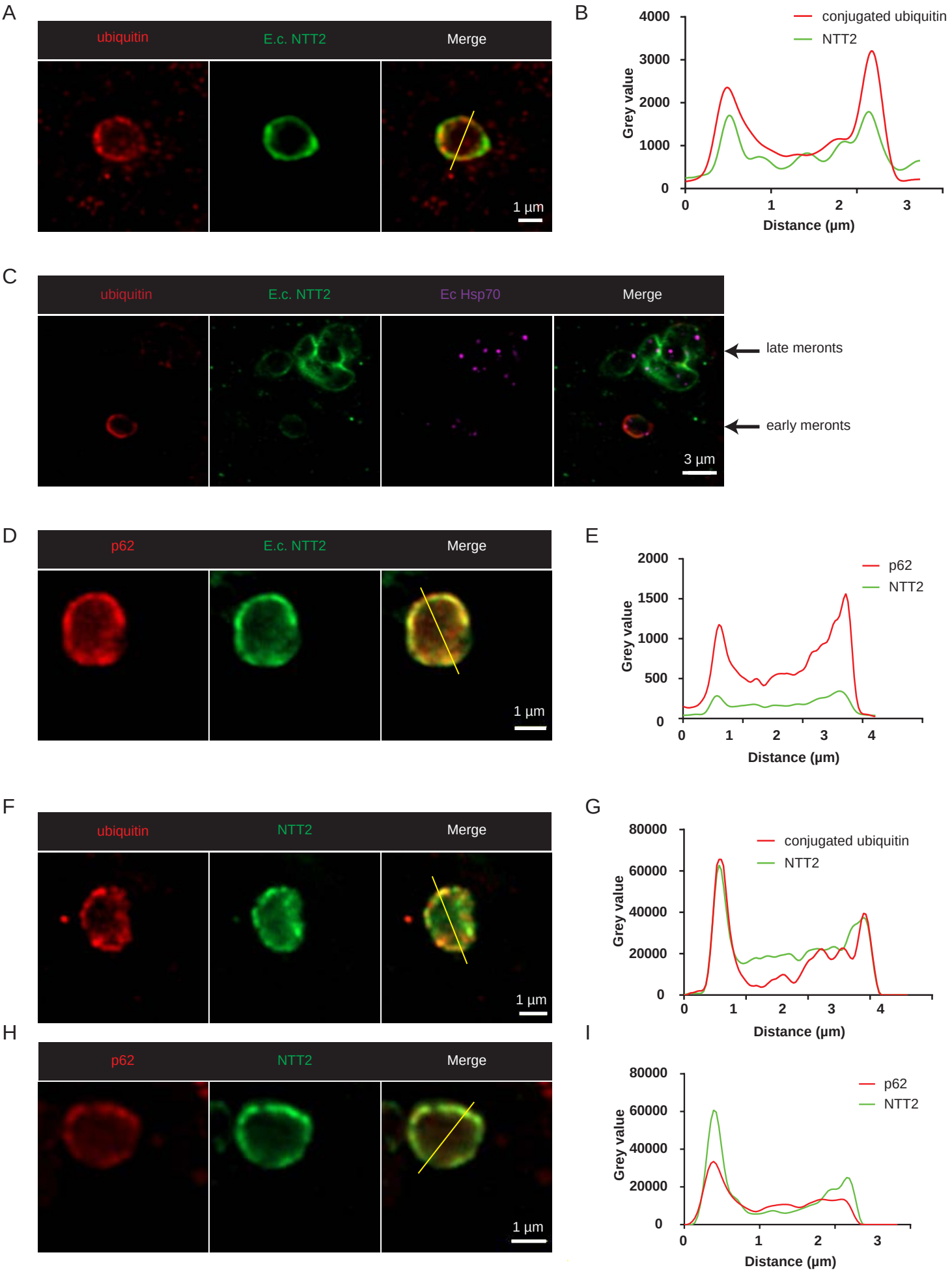
A
ubiquitin
E.c. NTT2
Merge
1 µm
B
conjugated ubiquitin
NTT2
Grey value
Distance (µm)
C
ubiquitin
E.c. NTT2
Ec Hsp70
Merge
late meronts
early meronts
3 µm
D
p62
E.c. NTT2
Merge
1 µm
E
p62
NTT2
Grey value
Distance (µm)
F
ubiquitin
NTT2
Merge
1 µm
G
conjugated ubiquitin
NTT2
Grey value
Distance (µm)
H
p62
NTT2
Merge
1 µm
I
p62
NTT2
Grey value
Distance (µm)

Figure 2

A

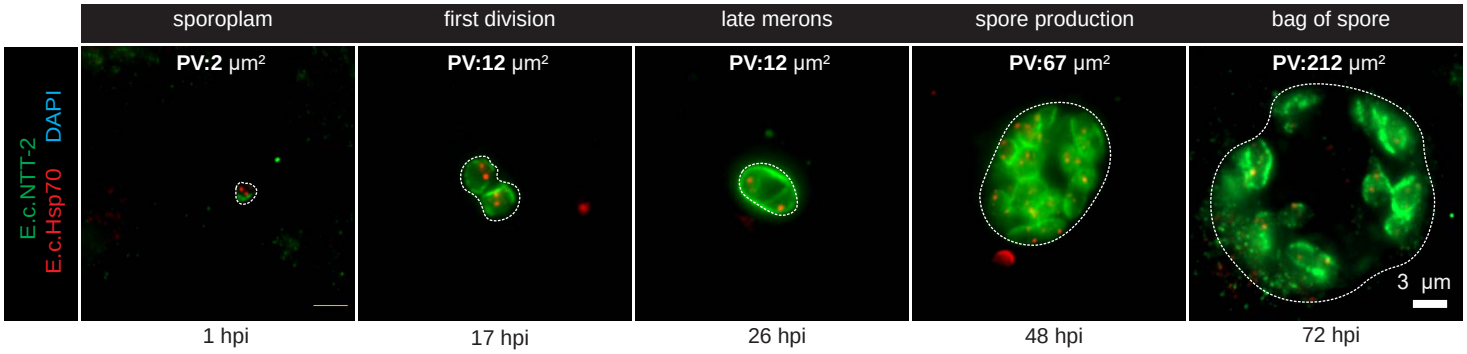

B

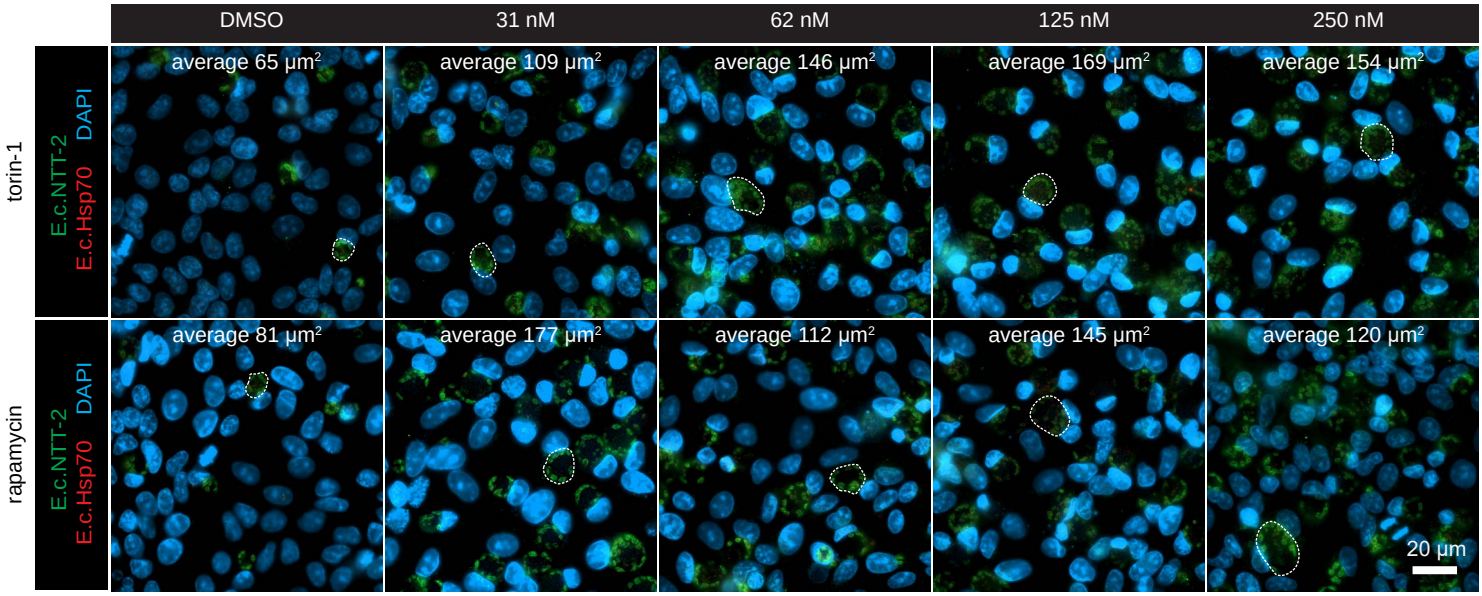

C

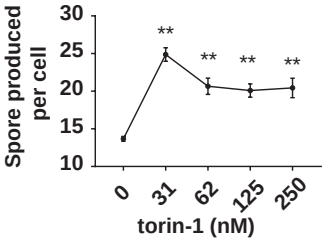

D

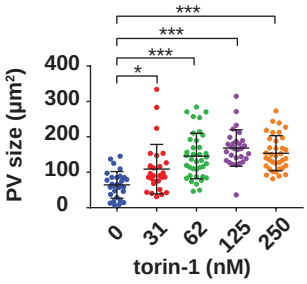

E

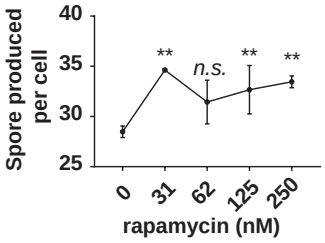

F

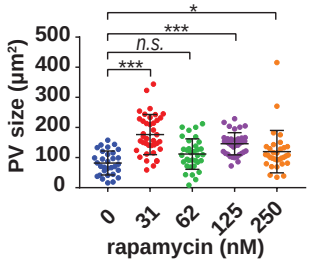

G

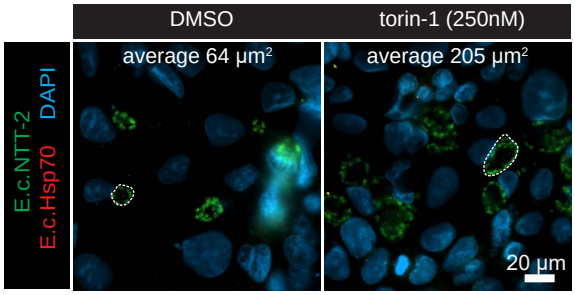

H

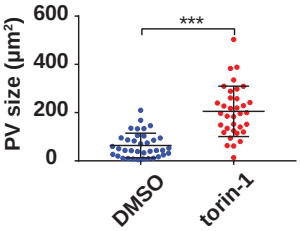

I

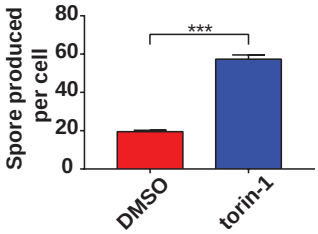

J

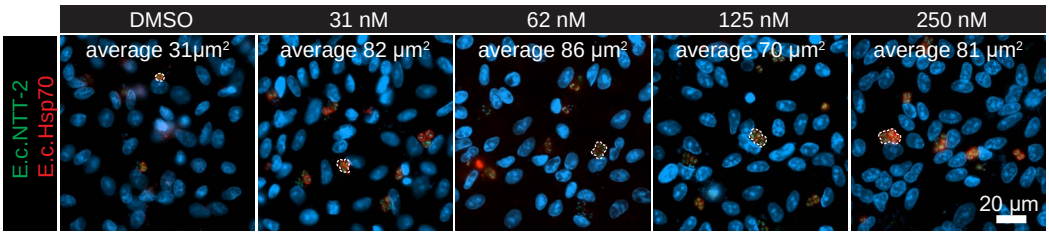

K

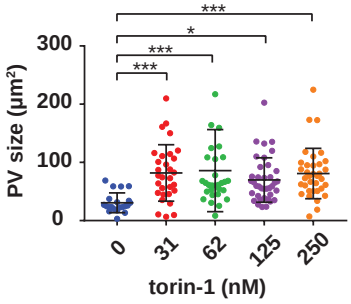

Figure 3

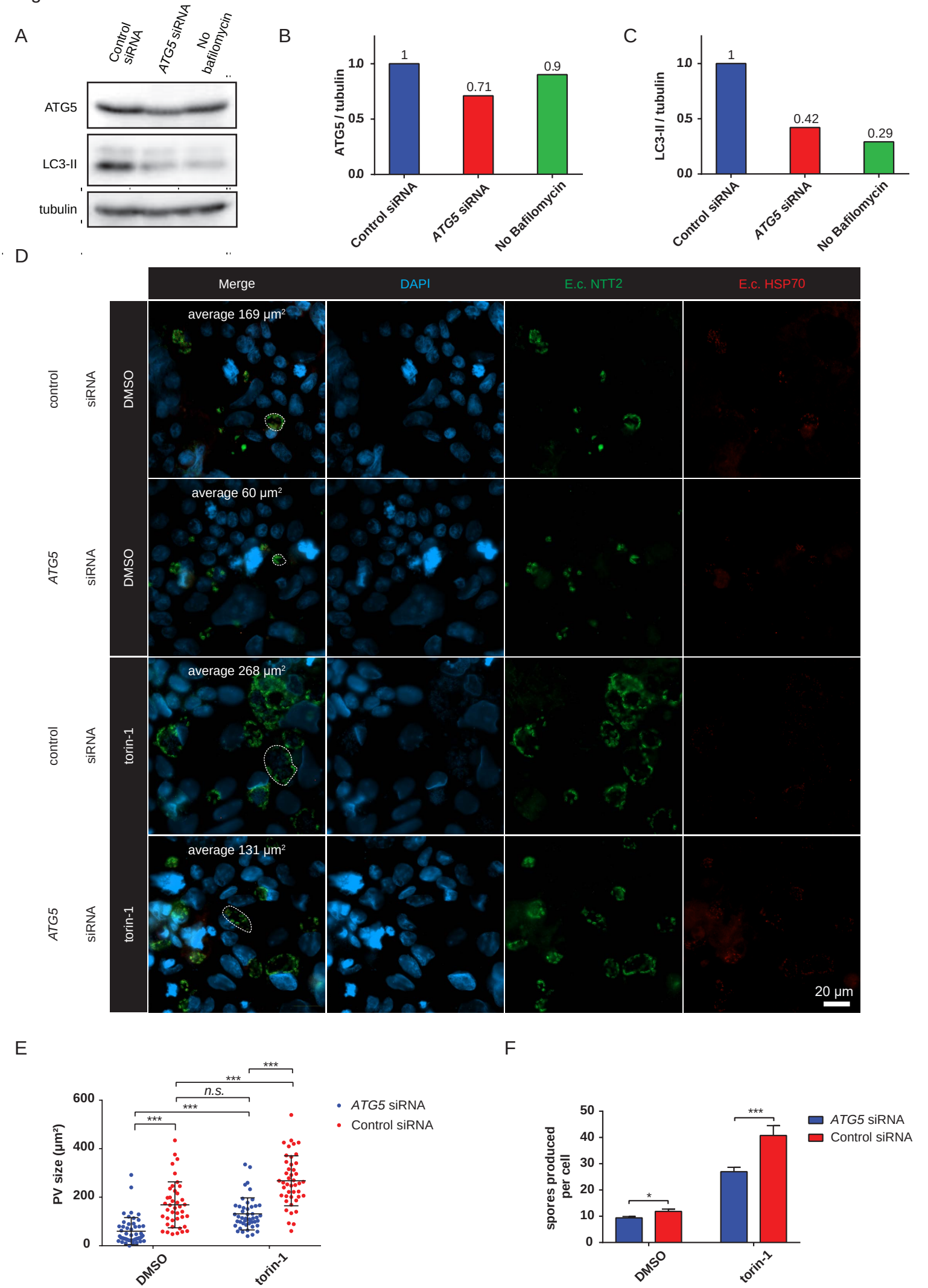
A
Control siRNA
ATG5 siRNA
No bafilomycin
ATG5
LC3-II
tubulin
B
ATG5 / tubulin
1.0
0.5
0.0
1
0.71
0.9
Control siRNA
ATG5 siRNA
No Bafilomycin
C
LC3-II / tubulin
1.0
0.5
0.0
1
0.42
0.29
Control siRNA
ATG5 siRNA
No Bafilomycin
D
Merge
DAPI
E.c. NTT2
E.c. HSP70
control siRNA
DMSO
average 169 µm²
ATG5 siRNA
DMSO
average 60 µm²
control siRNA
torin-1
average 268 µm²
ATG5 siRNA
torin-1
average 131 µm²
20 µm
E
PV size (µm²)
600
400
200
0
***
***
n.s.
***
***
DMSO
torin-1
ATG5 siRNA
Control siRNA
F
spores produced per cell
50
40
30
20
10
0
*
***
DMSO
torin-1
ATG5 siRNA
Control siRNA

Figure 4

A

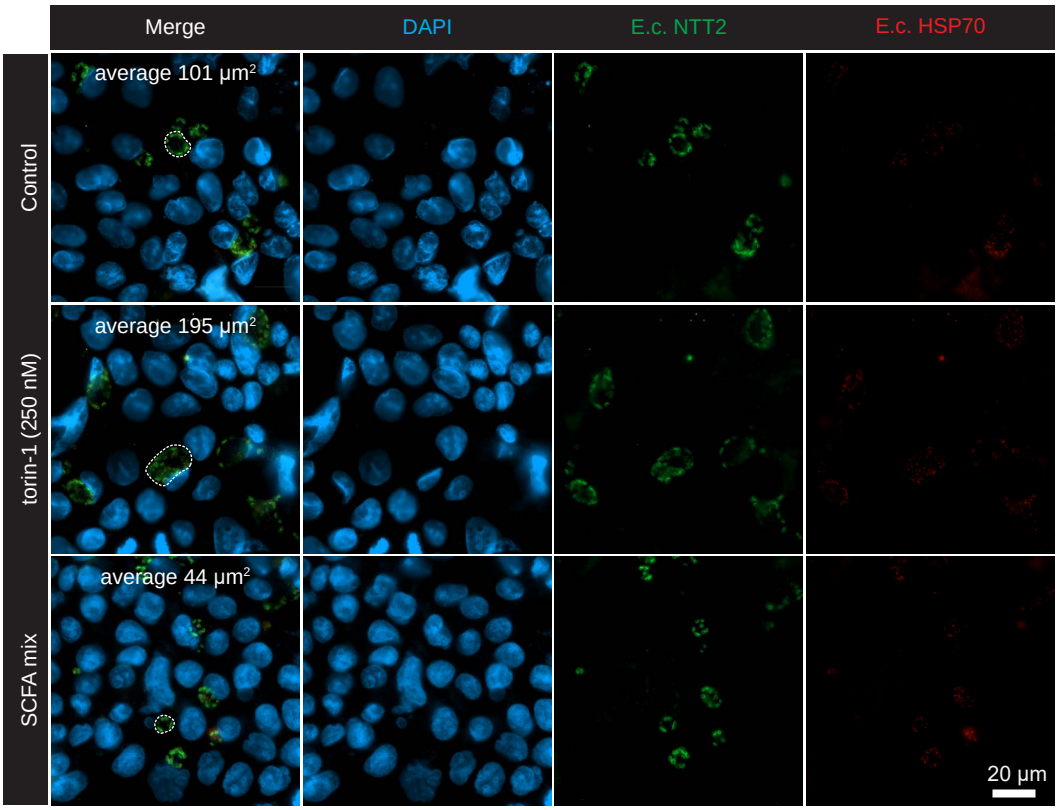
Merge
DAPI
E.c. NTT2
E.c. HSP70
Control
torin-1 (250 nM)
SCFA mix
average 101 µm²
average 195 µm²
average 44 µm²
20 µm

B

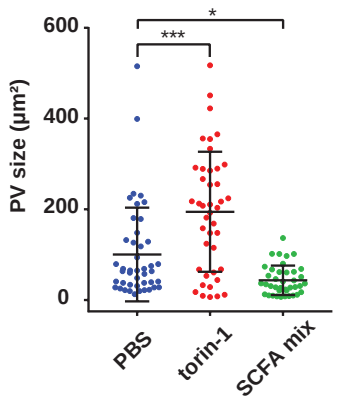
PV size (µm²)
600
400
200
0
*
***
PBS
torin-1
SCFA mix

C

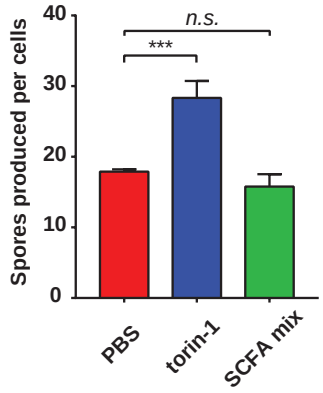
Spores produced per cells
40
30
20
10
0
n.s.
***
PBS
torin-1
SCFA mix